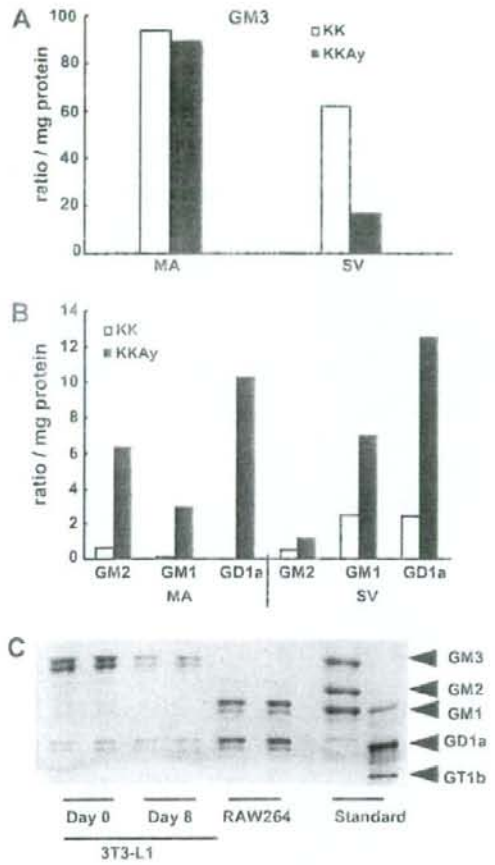

Fig. 4. Ganglioside profiles in cell fractions isolated from adipose tissues. (A,B) Perigonadal adipose tissue of KK and KKAy mice (pooled samples from four mice) were fractionated into stromal vascular cell (SV) fractions and mature adipocyte (MA) fractions. Gangliosides were extracted, purified and analyzed by HPLC/MS as in Fig. 2. (C) Gangliosides extracted from undifferentiated (Day 0) and differentiated (Day 8) 3T3-L1 cells and RAW264 macrophage were separated on TLC as described in Materials and methods.

ion-trap MS. A variety of methods of analyzing gangliosides have been reported. Standard HPLC methods identify and quantify oligosaccharide moieties that are released from gangliosides by digestion with ceramide glycanase [12]. Enzymatic digestion of a ganglioside leads to loss of the structural information on its ceramide moiety and a drawback for quantitative works, i.e., a difficulty in determining enzymatic conditions to ensure quantitative recovery of digested sugar chains. Furthermore, this method includes multiple processing steps and is laborious. On the other hand, HPLC/MS can separate an individual ganglioside molecular species and identify its sugar sequence and the structure of its ceramide moiety. Very recently the methods with MS and tandem MS combined with reverse-phase HPLC were applied to determine ganglioside profiles of glioblastoma cells [13] and mouse brain [14].

Adipose tissue contained a huge amount of triglycerides, and gangliosides as minor components. In our hands simple solvent partition methods were not suitable for extracting ganglioside from adipose tissues for MS measurements, because significant amounts of non-polar impurities were contaminated in ganglioside fractions. Hence, we used an anion-exchange column for enriching and purifying gangliosides and then purified ganglioside fractions were subjected to saponification under mild alkaline conditions to remove triacylglycerols and phospholipids almost completely. This resulted in breaking minor ester modification, e.g., an O-acetyl linkage on sugar groups, leading to missing these slightly modified forms. However, the amide linkage in N-glycolylneuraminyl moiety is preserved and we found that adipose GM3 in genetic obese models and all a-series gangliosides more complex than GM3 increased in obese adipose tissues prefer N-glycolylneuraminyl species.

In genetic, and diet-induced obese mice, adipose tissues contained abundant GM2, GM1, and GD1a, compared with each control group. A fractionation study showed that these gangliosides were increased in both adipocyte and SV fractions (Fig. 4A and B). The adipocyte fractions contain mature adipocytes, whereas SV contains pre-adipocytes and interstitial cells including resident and infiltrated macrophages. In SV fraction, expression of macrophage marker genes CD68 and F4/80 were significantly elevated in severely obese KKAy mice (Fig. 3D), indicating increased macrophage infiltration into the obese adipose tissues. Macrophage cell line contained significantly higher amount of GM1 and GD1a, compared to pre-adipocytes and mature adipocytes, like SV (Fig 4C). These results suggest that infiltrated macrophage could take part in the increased GM1 and GD1a levels in SV fraction. A previous in vitro study showed that a proinflammatory cytokine TNFα elicited both GM3 synthase expression and activity in 3T3-L1 adipocytes, suggesting that TNFα secreted from infiltrated macrophages could have a regulatory role in ganglioside synthase expression [7]. In contrast, this study shows the mRNA levels of GM2 synthase were significantly increased in the adipose tissues of DIO and KKAy mice, but not those of GM3 synthase (Fig. 3A and C). This suggests that the action of GM2 synthase directs the metabolic flow of a-series ganglioside towards GD1a. The exact roles played by gangliosides and cytokines secreted by infiltrated macrophages in obesity pathophysiology remain to be clarified.

In both DIO and genetic obesity models, the proportion of GM3 species with shorter chain acyl (16:0 and 18:0) moieties significantly increased, compared with each control group. It has generally been accepted that GM3 is enriched in lipid microdomain. GM3 is the major adipose gangliosides (Fig. 2A) and can take part in forming a scaffold of lipid microdomain. Shortening of GM3 acyl moieties causes an increase in membrane fluidity of the domains, which may perturb its functional integrity, leading to affecting signaling efficiency through lipid microdomain. In this connection, T cell-specific targeting of serine palmitoyltransferase gene caused loss of sphingolipids and shortening of their acyl moieties in detergent-resistant membrane fractions prepared from targeted thymocytes, which is associated with abnormal T cell differentiation in the thymus (H. Tojo, S. Osuka, unpublished results).

In summary, we demonstrated that obesity induced adipose a-series gangliosides downstream of GM3: GM2, GM1, and GD1a by normal-phase HPLC/MS. Functional analysis of these gangliosides will shed light on the pathophysiology of obesity-associated diseases.

Acknowledgments

This work was supported by Grants-in-Aid for Scientific Research from the Ministry of Education, Culture, Sports, Science, and Technology of Japan, and Ono pharmaceutical Research Grant.

Appendix A. Supplementary data

Supplementary data associated with this article can be found, in the online version, at doi:10.1016/j.bbrc.2008.12.086.

References

[1] A.W. Ferrante Jr., Obesity-induced inflammation: a metabolic dialogue in the language of inflammation, J. Intern. Med. 262 (2007) 408–414.

[2] S.P. Weisberg, D. McCann, M. Desai, M. Rosenbaum, R.L. Leibel, A.W. Ferrante Jr., Obesity is associated with macrophage accumulation in adipose tissue, J. Clin. Invest. 112 (2003) 1796–1808.

[3] S.P. Weisberg, D. Hunter, R. Huber, J. Lemieux, S. Slaymaker, K. Vaddi, I. Charo, R.L. Leibel, A.W. Ferrante Jr., CCR2 modulates inflammatory and metabolic effects of high-fat feeding, J. Clin. Invest. 116 (2006) 115–124.

[4] G. Van Echten, K. Sandhoff, Ganglioside metabolism. Enzymology, topology, and regulation, J. Biol. Chem. 268 (1993) 5341–5344.

[5] S. Hakomori, Bifunctional role of glycosphingolipids. Modulators for transmembrane signaling and mediators for cellular interactions, J. Biol. Chem. 265 (1990) 18713–18716.

[6] T. Yamashita, A. Hashiramoto, M. Haluzik, H. Mizukami, S. Beck, A. Norton, M. Kono, S. Tsuji, J.L. Daniotti, N. Werth, R. Sandhoff, K. Sandhoff, R.L. Proia, Enhanced insulin sensitivity in mice lacking ganglioside GM3, Proc. Natl. Acad. Sci. USA 100 (2003) 3445–3449.

[7] S. Tagami, J. Inokuchi Ji, K. Kabayama, H. Yoshimura, F. Kitamura, S. Uemura, C. Ogawa, A. Ishii, M. Saito, Y. Ohtsuka, S. Sakaue, Y. Igarashi, Ganglioside GM3 participates in the pathological conditions of insulin resistance, J. Biol. Chem. 277 (2002) 3085–3092.

[8] T. Pacuszka, J. Moss, P.H. Fishman, A sensitive method for the detection of GM1-ganglioside in rat adipocyte preparations based on its interaction with choleragen, J. Biol. Chem. 253 (1978) 5103–5108.

[9] M. Ito, U. Tchoua, M. Okamoto, H. Tojo, Purification and properties of a phospholipase A2/lipase preferring phosphatidic acid, bis(monoacylglycerol) phosphate, and monoacylglycerol from rat testis, J. Biol. Chem. 277 (2002) 43674–43681.

[10] Y. Nagatsuka, H. Tojo, Y. Hirabayashi, Identification and analysis of novel glycolipids in vertebrate brains by HPLC/mass spectrometry, Methods Enzymol. 417 (2006) 155–167.

[11] S.K. Kundu, D.D. Scott, Rapid separation of gangliosides by high-performance liquid chromatography, J. Chromatogr. 232 (1982) 19–27.

[12] J.M. Aerts, R. Ottenhoff, A.S. Powlson, A. Grefhorst, M. van Eijk, P.F. Dubbelhuis, J. Aten, F. Kuipers, M.J. Serlie, T. Wennekes, J.K. Sethi, S. O'Rahilly, H.S. Overkleeft, Pharmacological inhibition of glucosylceramide synthase enhances insulin sensitivity, Diabetes 56 (2007) 1341–1349.

[13] H. He, C.A. Conrad, C.L. Nilsson, Y. Ji, T.M. Schaub, A.G. Marshall, M.R. Emmett, Method for lipidomic analysis: p53 expression modulation of sulfatide, ganglioside, and phospholipid composition of U87 MG glioblastoma cells, Anal. Chem. 79 (2007) 8423–8430.

[14] K. Ikeda, T. Shimizu, R. Taguchi, Targeted analysis of ganglioside and sulfatide molecular species by LC/ESI-MS/MS with theoretically expanded multiple reaction monitoring, J. Lipid Res. 49 (2008) 2678–2689.

International Immunology, Vol. 20, No. 11, pp. 1427–1437
doi:10.1093/intimm/dxn100

Impaired TCR signaling through dysfunction of lipid rafts in sphingomyelin synthase 1 (*SMS1*)-knockdown T cells

Zhe-Xiong Jin[1], Cheng-Ri Huang[1], Lingli Dong[1,2], Seiji Goda[3], Takafumi Kawanami[1], Toshioki Sawaki[1], Tomoyuki Sakai[1], Xiao-Peng Tong[1], Yasufumi Masaki[1], Toshihiro Fukushima[1], Masao Tanaka[1], Tsuneyo Mimori[4], Hiromasa Tojo[5], Eda T. Bloom[6], Toshiro Okazaki[7] and Hisanori Umehara[1]

[1]Department of Hematology and Immunology, Kanazawa Medical University, 1-1 Daigaku, Uchinada, Ishikawa 920-0293, Japan
[2]Department of Hematology and Immunology, Tongji Hospital, Huazhong University of Science and Technology, Wuhan, Hubei 430030, China
[3]Department of Biochemistry, Osaka Dental University, Kuzuha, Osaka, Japan
[4]Department of Rheumatology and Clinical Immunology, Kyoto University Graduate School of Medicine, Sakyo-ku, Kyoto 606-8507, Japan
[5]Department of Biochemistry and Molecular Biology, Osaka University Graduate School of Medicine, Osaka 565-0871, Japan
[6]Division of Cellular and Gene Therapies (HFM-725), Center for Biologics Evaluation and Research, Food and Drug Administration, Bethesda, MD 20892, USA
[7]Department of Clinical Laboratory, Medicine/Hematology, Faculty of Medicine, Tottori University, Yonago, Tottori 683-8504, Japan

Keywords: LAT, lipid rafts, microdomain, sphingomyelin, TCR

Abstract

During T cell activation, TCRs cluster at the center of the T cell–antigen-presenting cell interface forming the central supramolecular activation cluster. Although it has been suggested that sphingolipid- and cholesterol-rich microdomains, termed lipid rafts, form platforms for the regulation and transduction of TCR signals, an actual role for membrane sphingomyelin (SM), a key component of lipid rafts, has not been reported. After cloning a gene responsible for SM synthesis, sphingomyelin synthase (SMS) 1, we established a SM-knockdown cell line (Jurkat-SMS1/kd) by transfection of SMS1-short-interfering RNA into Jurkat T cells, which is deficient in membrane expression of SM. Upon CD3 stimulation, expression of CD69 (the earliest leukocyte activation antigen), activation-induced cell adhesion and proliferation as well as TCR clustering was severely impaired in Jurkat-SMS1/kd cells. CD3-induced tyrosine phosphorylation and association of linker for activation of T cell with *ZAP-70* and Grb2 and phosphorylation of protein kinase C (PKC) θ were also severely impaired in Jurkat-SMS1/kd cells. Finally, translocation of TCR, *ZAP-70* and PKCθ into lipid rafts was markedly decreased in Jurkat-SMS1/kd cells. These findings indicate that membrane SM is crucial for TCR signal transduction, leading to full T cell activation through lipid raft function.

Introduction

Sphingolipid- and cholesterol-rich microdomains, termed lipid rafts, play a key role in protein sorting (1). They have been implicated in the cytoskeletal re-organization that forms platform immunological synapses at the cell membrane, which are involved in signal transduction, for example of signals originating through the TCR (2–4). Since the lipid raft-resident molecules such as *src* family kinases and ganglioside GM1 relocalize toward the immunological synapse, it appears that the immunological synapse could be described as a merger of lipid rafts (5, 6).

The stimulation on TCR and CD3 complexes induces a series of signal transduction events leading to activation of cytosolic protein tyrosine kinases (PTKs) such as *lck* and *ZAP-70*. Activated *ZAP-70* phosphorylates the transmembrane adaptor protein linker for activation of T cells (LATs). LAT consists of primarily cytoplasmic region with two cysteine residues

Correspondence to: H. Umehara; E-mail: umehara@kanazawa-med.ac.jp

Transmitting editor: K. Okumura

Received 28 June 2008, *accepted* 11 August 2008

Advance Access publication 26 September 2008

just below the transmembrane region and is targeted to lipid rafts by palmitoylation of cysteines (7). Tyrosine phosphorylated LAT, via phosphotyrosine-based docking motifs, recruits SH2 domain-containing signaling proteins, including SLP-76, phospholipase Cγ (PLC-γ), phosphatidylinositol 3 kinase (PI3K) and Grb2 etc., and allows subsequent extension of the signaling scaffold (8).

Another important pathway for T cell activation different from tyrosine kinase cascade is the signal scaffolding of CARMA1 (caspase recruitment domain, CARD, membrane-associated guanylate kinase, MAGUK, protein 1) and translocation of protein kinase C (PKC) θ into lipid rafts. Among the PKC isoforms, PKCθ, a Ca^{2+}-independent PKC isoform, is a critical component for TCR-induced NF-κB activation, because mice deficient for PKCθ show impaired activation of NF-κB (9), and PKCθ is selectively expressed in T cells and translocates to lipid rafts during antigen-receptor triggering (10). Taken together, these data support an important role for lipid rafts in TCR-mediated protein sorting and signal transduction.

In addition to these biochemical events, lipid rafts are implicated in the formation of the immunological synapse, where spatial organization and compartmentalization of membrane-associated proteins such as the TCR–CD3 complex, PTKs and adaptor molecules occur (8, 11). Immunological synapse formation with the central supramolecular activation cluster (cSMAC) depends on TCR-mediated signaling that induces the re-organization of the cytoskeleton and cell surface receptors, and the immunological synapse mediates effector functions. However, recent imaging analyses such as single-particle tracking, fluorescence resonance energy transfer (FRET) microscopy, FRET microscopy with fluorescence recovery after photobleaching and total internal reflection fluorescence microscopy reveal that TCR microclusters form prior to immunological synapses, are the site for antigen recognition and T cell activation and are continuously generated at the periphery of immunological synapses but are not accompanied by lipid raft clustering (12–14). Thus, the functional roles of the immunological synapses and lipid rafts for the spatial-temporal organization of the enzymatic events during signaling are controversial.

Lipid rafts have been detected using cholera toxin B (CTx) which binds to ganglioside GM1 co-localized in rafts, and the role of rafts has been evaluated by disruption of rafts using the cholesterol-chelating reagent, methyl-β-cyclodextrin (MβCD). However, there has been no direct evidence that membrane sphingomyelin (SM) is involved in raft functions and TCR-mediated signal transduction due to the lack of molecular cloning of the sphingomyelin synthase (SMS) gene and of a specific probe to membrane SM. Previously, we and others have succeeded in cloning the human cDNA for *SMS1* (15, 16). Using SM synthesis-deficient cells and cells in which function has been restored by transfection with *SMS1* gene, we have reported that membrane SM plays a key role in Fas-mediated apoptosis through its involvement in the efficient clustering of Fas and lipid rafts (17).

We herein report the establishment of a membrane SM-deficient cell line (Jurkat-SMS1/kd) by transfection of SMS1-short-interfering RNA (siRNA) into Jurkat T cells, and provide data demonstrating the role of membrane SM on T cell functions and CD3-activated signal pathways.

Methods

Antibodies and reagents

The human CD3ε-specific mAb, OKT3 (IgG_{2a}), was purchased from Biodesign International a custom ascites. The antibodies to anti-PKCθ, anti-Grb2, anti-LAT, anti-*lck*, anti-TCRβ and FITC-conjugated goat anti-rabbit IgG2a were purchased from Santa Cruz Biotechnology. Anti-phospho-PKCθ (Thr538) was purchased from Cell Signaling Technology (Beverly, MA, USA). Anti-TCRβF1 antibody was purchased from PIERCE ENDOGEN a Perbio Science (Rockford, IL, USA), anti-*ZAP-70* and anti-phosphotyrosine (4G10) antibody were purchased from Upstate Cell Signaling (Lake Placid, NY, USA). Rabbit anti-MBP anti-serum was purchased from New England BioLabs (Beverly, MA, USA). PE-conjugated anti-human CD2, CD3, CD4, CD69, CD95 and anti-human TCRγβ antibody were purchased from BD Bioscience (San Jose, CA, USA). Lysenin, goat anti-mouse IgG, FITC-conjugated CTx, HRP-conjugated CTx, PE-conjugated rabbit anti-mouse IgG, FITC-conjugated anti-rabbit IgG were purchased from Sigma–Aldrich (St Louis, MO, USA). The cell viability assay kit (WST-8) was purchased from Wako Co. Ltd (Kyoto, Japan). L-[U-^{14}C] serine was purchased from Amersham Biosciences (Piscataway, NJ, USA). The ECL immunodetection system, HRP-conjugated goat anti-mouse and anti-rabbit IgG mAb were obtained from Amersham International (Amersham, Bucks, UK).

Construction of human SMS1-siRNA vector

The sequences of siRNA for human *SMS1* genes and the control (scrambled sequence (SCR)) were designed by siRNA Design Support System (Takara Bio, Shiga, Japan). The sequences are as follows: *SMS1*, GCCCAACTGCGAAGAATAA (seq. #6) and SCR, ATTGAAAAAGACACGCGCC (temporally designated SMS negative). Based on these sequences, 'top (T)' and 'bottom (B)' pairs of oligonucleotides were synthesized as follows: *SMS1*-RNAi6-T (for *SMS1*), GATCCGCCCAACTGCGAAGAATAATTCAAGAGATTATTCTTCGCAGTTGGGCTTTTTTAT; *SMS1*-RNAi6-B (for *SMS1*), CGATAAAAAAGCCCAACTGCGAAGAATAATCTCTTGAATTATTCTTCGCAGTTGGGCG; SMSneg-RNAi-T (for SCR), GATCCATTGAAAAAGACACGCGCCTTCAAGAGAGGCGCGTGTCTTTTTCAATTTTTTTAT and SMSneg-RNAi-B (for SCR), CGATAAAAAAATTGAAAAAGACACGCGCCTCTCTTGAAGGCGCGTGTCTTTTTCAATG. The 'T' and 'B' pairs of oligonucleotides were annealed and ligated into *Bam*HI and *Cla*I sites of pSINsi-hU6 (Takara Bio) according to the manufacturer's instruction. The ligation was confirmed by digestion with *Bam*HI and *Bln*I (performed 40127-40129 and 40330 for *SMS* and SCR, respectively). The resultant vectors were designated pSINsi-*SMS1* and SCR, respectively, and transfected into Jurkat T cells via retroviral particles.

Cell transfection and establishment of SM-knockdown Jurkat T cells

Production of the retrovirus carrying the *SMS1*-siRNA and SCR-siRNA as well as infection by the recombinant viruses were performed as previously reported (18). Cells were selected with 1–3 mg ml^{-1} G418 for several weeks and then

separated into single cells by limiting dilution. The isolated clones showing the most suppression of *SMS1* level (Jurkat-SMS1/kd) and control (Jurkat-SM+) were chosen for further experiments.

Measurement of the SMS1-expression level by real-time PCR

Total RNA was isolated from Jurkat-SM+ and Jurkat-SMS1/kd cells using QIAGEN RNeasy kit (QIAGEN, MD, USA) and the cDNA was synthesized using first-strand cDNA synthesis kit (Life Sciences). Open reading frame sequences of SMS cDNA were amplified using Pyrobest DNA polymerase (Takara Bio) and primers *SMS1*-F4 (TGTCCTGCCAAGAGAGAGC) and *SMS1*-R1 (TGGAGTTCTTAGCACTTCGG) for *SMS1* (PCR performed: 40311), *SMS2*-F5 (ACAAGAACTTGACCATCTCC) and *SMS2*-R4 (TTGCTCCTCAGGTCGATTTC) for *SMS2* (PCR performed: 40122) and *SMS3*-F2 (AGCTGAGGCTGAGGAGAG) and *SMS3*-R4 (CATCCAATTAGTCTTTTCATTATTG) for *SMSr* (PCR performed: 40122). As a control, human glyceraldehyde 3-phosphate dehydrogenase (GAPDH) mRNA was analyzed using primers GAPDH-F (CAACGGATTTGGTCGTATT, upstream) and GAPDH-R (CACAGTCTTCTGGGTGGC, downstream). In 2 μl of the synthesized DNA, 2 premix (10 μl), up- and downstream primers of GAPDH (1 μl of each) were added sequentially, with the total volume adjusted to 20 μl with triple distilled water. The mixture was loaded in a 7500 real-time PCR system (Applied Biosystem) and pre-denaturation at 94°C for 5 min, 35 cycles of denaturation at 94°C for 30 s, annealing at 55°C for 30 s and extension at 72°C for 30 s were carried out, followed by a final extension at 72°C for 7 min. The PCR (real-time form) production of the DNA copy base pairs was computed by Avogadro's number system.

FACS analyses

To detect SM localized at the outer leaflet of the plasma membrane, cells were stained on ice for 30 min with non-toxic lysenin fused to maltose-binding protein (MBP-lysenin) (19), followed with rabbit anti-MBP anti-serum (New England BioLabs) and FITC-conjugated anti-rabbit IgG (Sigma–Aldrich) and analyzed with a FACS Calibur (Becton Dickinson, Mountain View, CA, USA). Surface expressions of ganglioside GM1 and cholesterol were analyzed using FITC-conjugated CTx (Sigma–Aldrich) and a fluorescein ester of poly(ethyleneglycol)-derivatized cholesterol ether (PEG-Chol) (20), respectively. Data were analyzed using Cell Quest software (Becton Dickinson).

Confocal microscopy

For visualization of SM localized at the outer leaflet of plasma membrane, cells were allowed to settle onto slides coated with poly-L-lysine, fixed in 4% formaldehyde, stained with lysenin-MBP at 4°C for 20 min, followed with anti-MBP mAb and FITC-conjugated anti-mouse IgG mAb. Cells were also stained with PE-conjugated anti-human αβTCR antibody or FITC-conjugated CTx subunit. Fluorescence was detected with a confocal microscope (Zeiss LSM-5 Pascal laser scan, Carl Zeiss, Oberkochen, Germany) equipped (21).

To assess the co-localization of TCR, SM and ganglioside GM1, cells were stained with 5 μg ml^{-1} of anti-CD3 antibody (OKT3) at 4°C for 15 min. After washing, cells were warmed up to 37°C in a water bath and cross-linked with 10 μg ml^{-1} of anti-mouse IgG antibody for 5 min. Cells were fixed with 4% paraformaldehyde for 20 min at 22 °C and mounted in FITC-conjugated secondary antibody. Large clusters of TCR were defined as cells in which the fluorescence condenses onto >25% of the cell surface, whereas fluorescence was homogenously distributed on the membrane of non-stimulated cells. In each experiment, a blinded observer counted 150–200 cells, and a second independent observer confirmed the count.

Cell adhesion and migration assays

Adhesion and migration assays with Jurkat-SMS1/kd and Jurkat-SM+ cells were performed using calcein–acetoxymethyl ester labeling of cells described as previously (22). Adhesion assays were performed in flat-bottomed 96-well plates (Costar, Cambridge, MA, USA) pre-coated with 0.3 μg per well fibronectin (FN) and blocked with PBS supplemented with 2.5% BSA (23). Cells were re-suspended in PBS supplemented with 0.5% human serum albumin (PBS/HSA) at 1.6×10^6 cells ml^{-1} after Ficoll separation. For CD3 stimulation, cells were pre-incubated on ice for 30 min with OKT3 mAb and then washed twice with PBS/HSA. After washing, 80 000 cells per well were added to the appropriate wells. The following stimulating agents were added to the wells before the addition of cells: 10 ng ml^{-1} phorbol myristate acetate (PMA) or 1 μg ml^{-1} of goat anti-mouse IgG (for CD3 stimulation). Cells were incubated at 4°C for 1 h, plates were floated in a 37°C water bath for the indicated times and non-adherent cells were removed by washing and fluorescence was measured as described previously (24).

Migration assays were performed in transwell chambers with 3-mm polycarbonate membrane (Corning Incorporated) pre-coated with 100 μg ml^{-1} FN or inter cellular adhesion molecules-1 (ICAM-1) on both sides of the filter. Human stromal cell-derived factor 1α (CXCL12) was diluted to appropriate concentrations in medium and added to the lower chamber of the transwell chambers. The cells were allowed to migrate for 4 h at 37°C in 5% CO_2. Each sample was assayed in triplicate, and migrated cells were counted in five randomly selected high-power fields (×400) per well. Results were expressed as mean ± SD per mm^2 from one representative experiment.

Cell labeling, lipid separation and ceramide measurement

For detection of SM synthesis, cells were re-seeded at 5×10^5 cells ml^{-1} in the RPMI-1640 medium with 2% FBS and L-[^{14}C] serine (specific activity; 155 mCi mmol^{-1}) and incubated at 37°C in 5% CO_2 for 36 h. The cell lipids were extracted, applied to silica gel thin-layer chromatography (TLC) plates (Whatman, Maidstone, UK) and developed as described previously (25). Radioactivity within spots of ceramide-1-phosphate was estimated with a BASE III image analyzer system (Fuji Photo Film, Kanagawa, Japan) and expressed as photo-stimulated luminescence arbitrary units (26).

HPLC/mass spectrometric analysis

To assess the amounts and molecular species compositions of SM in the *SMS1*-deficient cells, we used normal-phase

HPLC/ion-trap mass spectrometry (27, 28). Lipid extracts were prepared from cell pellets supplemented with appropriate amounts of myrisoyl ceramide, lauroyl glucosylceramide, lauroyl lactosylceramide and lauroyl SM as internal standards, evaporated under N_2 and dissolved in hexane/2-propanol (3:2). To remove the majority of ester-containing lipids, an aliquot was hydrolyzed at a mild alkaline pH and 60°C for 60 min, extracted by the Bligh and Dyer method, evaporated and finally dissolved in the previous solvent. An aliquot (1–2 μl) of the extracts was directly subjected to HPLC/mass spectrometry. Sphingolipids were separated into their classes and subclasses in the order from lower to higher polarity on a trap and separation silica columns connected in series (Fortispack of 1–20 mm and 1–100 mm, OmniSeparo-TJ, Inc., Hyogo, Japan). Effluents were monitored with an LCQdeca-XP mass spectrometer interfacing with an XYZ stage equipped with a fluoropolymer-coated electrospray tip, FortisTip (OmniSeparo-TJ, Inc.) of 150 μm in outer diameter/20 μm in inner diameter. Sphingolipids were identified with the mass-to-charge ratio (*m/z*) values and data-dependent, first or second-stage tandem mass spectrometry (MS/MS or MS^3) and quantified based on comparison of peak areas on chromatograms of target and internal standard ions of the same class. Peak area values were corrected for the contributions of natural abundance ^{13}C isotope, i.e. the difference between the carbon numbers of a target and an internal standard molecule and the overlapping of ions with 2 ^{13}C isotopes replaced in molecular ions with 2-amu lower mass (29).

Immunoprecipitation, western blotting and immunoblotting

Cells were solubilized with lysis buffer containing 50 mM Tris–HCl, pH 7.6, 1% Brij 97, 300 mM NaCl, 5 mM EDTA, 10 μg ml^{-1} leupeptin, 10 μg ml^{-1} aprotinin, 1 mM phenylmethylsulfonyl fluoride (PMSF) and 1 mM sodium orthovanadate with gentle rocking for 30 min at 4°C. Immunoprecipitated proteins were fractionated by SDS–PAGE (8–12% polyacrylamide gels), electrophoretically transferred to membranes and blotted with antibodies as indicated. Peroxidase-conjugated secondary antibodies (Amersham) were used at a 1:1000 dilution and immunoreactive bands were visualized using ECL (Amersham) (26). Densitometry of the protein bands was performed using NIH image software (30). Quantitation of bands was corrected to the density of ganglioside GM1 and depicted as arbitrary units.

Isolation of a raft fraction in equilibrium density gradients

Raft fractions from 2.5 × 10^6 cells were prepared as described by Rodgers and Rose with minor modifications (21). In brief, 2.5 × 10^5 cells were lysed with 0.8 ml MS-buffered saline (MBS, 25 mM MES, pH 6.5, and 150 mM NaCl) containing 1% Triton X-100, 10 μg ml^{-1} leupeptin, 10 μg ml^{-1} aprotinin, 1 mM PMSF, 1 mM sodium orthovanadate and 5 mM EDTA. The lysate was homogenized with 10 strokes of a Dounce homogenizer (IWAKI Glass Co.), gently mixed with an equal volume of 80% sucrose (wt/vol) in MBS and placed in the bottom of a 14 × 89 mm clear centrifuge tube (model 344096; Beckman Coulter). The sample was then overlaid with 5.2 ml of 30% sucrose and 2.8 ml of 5% sucrose in MBS and centrifuged at 41 000 r.p.m. (rotor model SW41Ti; Beckman Coulter, Palo Alto, CA, USA) at 4°C for 21 h. After centrifugation, twelve 0.8-ml fractions (excluding the pellet) were collected from the top of the gradient. To examine the presence of cell surface and intracellular proteins in the density gradient fractions, 20 μl of each fraction was separated by SDS–(10–12%) PAGE and transferred to immobilon polyvinylidene difluoride membranes (Millipore, Bedford, MA, USA) for standard western blot analysis.

Assay for SMS activity

SMS1 activity assays were performed as described previously (15). Briefly, cells were homogenized in an ice-cold buffer containing 20 mM Tris–HCl, pH 7.4, 2 mM EDTA, 10 mM EGTA, 1 mM PMSF and 2.5 μg ml^{-1} leupeptin. The lysates containing 500 μg of cell protein were added to a reaction solution containing 10 mM Tris–HCl, pH 7.5, 1 mM EDTA, 20 μM C6-NBD-ceramide, 120 μM phosphatidyl choline and incubated at 37°C for 30 min. The lipids were extracted by the method of Bligh and Dyer, applied on the TLC plates and developed with solvent containing chloroform/methanol/12 mM $MgCl_2$ in H_2O (65:25:4) (31). The fluorescent lipids were visualized with a FluoroImager SI system (Amersham Biosciences). The radioactive spots were visualized using the BAS 2000 system.

Results

Establishment of membrane SM-knockdown cells (Jurkat-SMS1/kd)

After cloning the human cDNA-encoding *SMS1* (15), we established membrane SM-knockdown cell lines (Jurkat-SMS1/kd) and control cell lines (Jurkat-SM+) by transfection of Jurkat cells with *SMS1*- or control siRNAs followed by selection with geneticin and limiting dilution.

To examine the expression levels of *SMS1* gene in Jurkat-SMS1/kd and Jurkat-SM+ cells, we isolated total RNA from each cell line, and sense/anti-sense oligonucleotides for *SMS1*, *SMS2*, *SMSr* and GAPDH cDNAs were utilized to perform RT–PCR and real-time PCR. Results revealed that *SMS1* was a major SMS gene in Jurkat cells and that *SMS1* gene copy number was decreased in the Jurkat-SMS1/kd cells to ~60% of Jurkat-SM+ cells (Fig. 1A). To detect SMS1 enzyme activity, lipids were extracted from each cell lysates, and ceramide mass measurement was performed by diacylglycerol kinase assay (25). The enzyme activity in Jurkat-SMS1/kd cells was decreased to ~60% of that in Jurkat-SM+ cells (Fig. 1B). We next examined the overall lipid composition of Jurkat-SMS1/kd and Jurkat-SM+ cells using HPLC and mass spectrometric analysis. Jurkat-SMS1/kd cells displayed only a minor (up to 23%) reduction in SM levels compared with Jurkat-SM+ cells, namely 2.8 versus 3.6 nmol mg^{-1} protein (Fig. 1C). Jurkat cells contain limited numbers of SM molecular species, such as C16:0, C16:1, C22:0, C24:0 and C24:1, where the symbols indicate the carbon number followed by a colon and the number of double bonds in the acyl group. SMS1 deficiency in Jurkat cells did not change the molecular species distribution in SM so much (Fig. 1C).

Lysenin is a SM-directed cytolysin purified from the earthworm, which specifically binds to membrane SM and

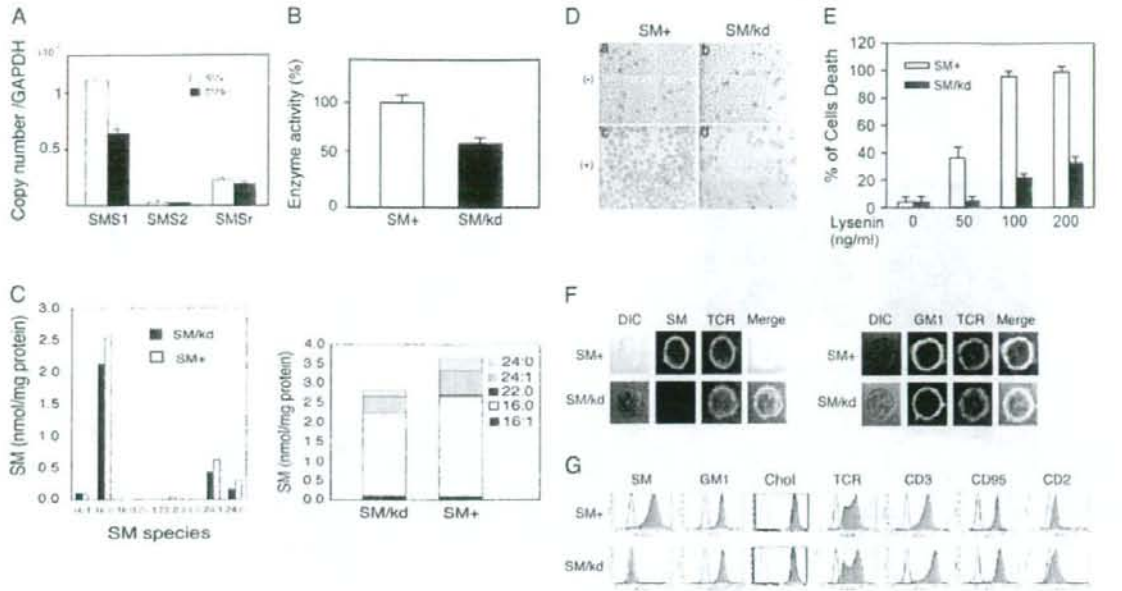

Fig. 1. SM-knockdown cells. (A) The *SMS1* gene expression. Expression levels of *SMS* genes were examined by RT-PCR and real-time PCR in Jurkat-SM+ and Jurkat-SMS1/kd cells. Each copy number was corrected to those of GAPDH. Results are representative of three experiments. (B) SMS1 enzyme activity in Jurkat-SM+ and Jurkat-SMS1/kd cells. Lipids were extracted from each cell lysate, and ceramide mass measurement was performed by the diacylglycerol kinase assay. Results are representative of three experiments. (C) Amounts of SM. Cell lipid extracts were prepared and subjected to liquid chromatography and electrospray ionization tandem MS as described under Methods. SM+, Jurkat-SM+ cells; SM/kd, Jurkat-SMS1/kd cells. (D) Microscopy of cells exposed to lysenin. Jurkat-SM+ cells (a and c) and Jurkat-SMS1/kd cells were treated in the presence (c and d) or absence (a and b) of 100 ng ml^{-1} of lysenin at 37 °C for 1 h and stained with 1% trypan blue. (E) Sensitivity against lysenin-mediated cell lysis. Cells were treated with the indicated concentration of lysenin at 37 °C for 1 h, then stained PI (propidium iodide) and analyzed by FACS scan. SM+, Jurkat-SM+ cells; SM/kd, Jurkat-SMS1/kd cells. Data are representative of three independent experiments. (F) Analysis of membrane SM expression by confocal microscopy. Cells were stained with lysenin-MBP and FITC-conjugated anti-mouse IgG mAb, PE-conjugated anti-TCR mAb or FITC-conjugated CTx. DIC, differential interference contrast; GM1, ganglioside GM1. (G) FACS analysis of membrane SM. To detect membrane SM, cells were stained with lysenin-MBP and FITC-conjugated anti-mouse IgG mAb. Surface expressions of ganglioside GM1 and cholesterol were analyzed using FITC-conjugated CTx and fPEG-Chol, respectively. Surface markers were analyzed with PE-conjugated anti-TCR, CD3, CD95 and CD2 mAbs. SM+, Jurkat-SM+ cells; SM/kd, Jurkat-SMS1/kd cells. Data are representative of more than five independent experiments.

induces pore formation in the plasma membrane and subsequent cell death (32, 33). We next examined the sensitivity to lysenin of Jurkat-SMS1/kd and Jurkat-SM+ cells (Fig. 1D). Cells were treated with 0, 50, 100 and 200 ng ml^{-1} of cytotoxic lysenin in the presence of 20 μg ml^{-1} of propidium iodide at room temperature for 15 min, and cell viability was analyzed with FACS. The results showed that Jurkat-SM+ cells underwent cell death after lysenin treatment in a dose-dependent manner with ~100% cell death at 100 ng ml^{-1} of lysenin, while Jurkat-SMS1/kd cells showed strong resistance (Fig. 1E).

Kiyokawa *et al.* (34) produced non-toxic lysenin by deleting N-terminal amino acids, which specifically binds to SM without induction of cell death. Using the mutant lysenin conjugated with MBP-lysenin, we examined the expression of membrane SM as well as expression of TCR on Jurkat-SMS1/kd and Jurkat-SM+ cells by confocal microscopy. Expression of TCR and ganglioside GM1, which is detected by CTx subunit and considered as a marker of lipid rafts, was detected equivalently on both cells. However, membrane SM was detected only on the surface of Jurkat-SM+ cells, but not on Jurkat-SMS1/kd cells (Fig. 1F). Next, we examined the expression of surface receptors and other membrane components such as CD3, CD95/Fas, CD2, αβTCR, ganglioside GM1 as well as membrane SM by FACS analysis. Membrane cholesterol partition was analyzed using fluorescein ester of fPEG-Chol as a probe (20). All markers except membrane SM were expressed at similar levels on both Jurkat-SMS1/kd and Jurkat-SM+ cells (Fig. 1G).

Role of membrane SM in clustering of TCR and lipid rafts

T cell stimulation induces formation of a large, multicomponent complex at the site of contact between T cells and antigen-presenting cell, termed the supramolecular activation complex or the immunological synapse (11, 35). This contact area of the T cell is highly enriched in lipid rafts or microdomains (5, 36). We examined the TCR clustering and co-localization with lipid rafts in Jurkat-SMS1/kd and Jurkat-SM+ cells using confocal microscopy. Full clustering of TCR and co-localization with TCR/lipid rafts were observed in Jurkat-SM+ cells after CD3 activation, but clustering in Jurkat-SMS1/kd cells was impaired (Fig. 2A) or diminished

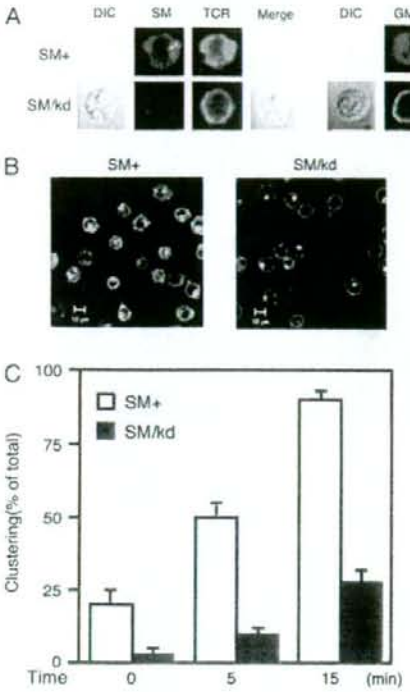

Fig. 2. Role of membrane SM in clustering of TCR and lipid rafts. (A) Confocal microscopy of membrane components after CD3 stimulation. Cells were stimulated with 5.0 μg ml^{-1} of CD3 mAb for 5 min and fixed with 1% paraformaldehyde for 10 min and fixed cells were incubated with FITC-labeled CTx (GM1), PE-conjugated anti-TCR and lysenin-MBP with FITC-conjugated anti-MBP (SM). (B) Confocal microscopy of TCR clustering. Cells were stimulated with 5.0 μg ml^{-1} of CD3 mAb for 5 min and fixed cells were incubated with FITC-conjugated anti-TCR. (C) Time kinetic study of TCR clustering. Cells were stimulated with 5.0 μg ml^{-1} of CD3 mAb for the indicated time and fixed cells were incubated with FITC-conjugated anti-TCR. Large clusters of TCR were defined as cells in which the fluorescence condenses onto >25% of the cell surface, whereas fluorescence was homogenously distributed on the membrane of non-stimulated cells. These data are representative of three independent experiments.

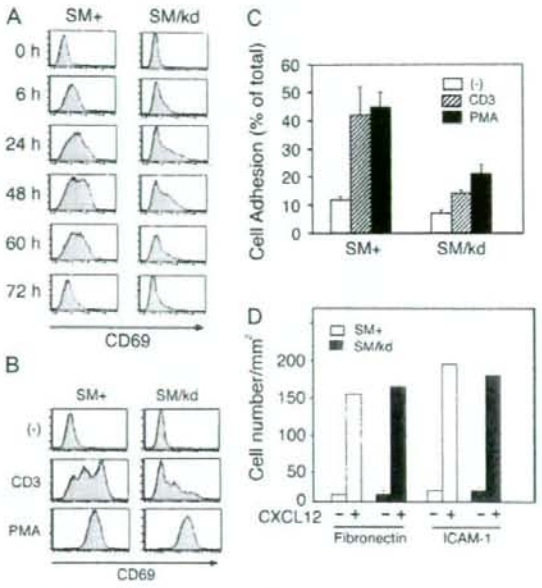

Fig. 3. Roles of membrane SM on CD3-mediated T cell activation. (A) Time kinetics of CD69 expression after CD3 stimulation. Cells were stimulated with 1 μg ml^{-1} of anti-CD3 mAb (OKT3) for the indicated time, and expression of CD69 was analyzed by FACS. (B) Effect of PMA on CD69 expression. Cells were stimulated with 1 μg ml^{-1} of OKT3 mAb or 2 ng ml^{-1} of PMA for 24 h and then expression of CD69 was assessed using FACS scan. (C) Cell adhesion to FN. Cells were labeled with calcein-acetoxymethyl ester. After CD3 activation or PMA stimulation, adhesion assays were performed in flat-bottomed 96-well plates pre-coated with 0.3 μg per well of FN. Data are expressed as % of total applied cells. (D) Cell migration to CXCL12. Migration assays were performed in transwell chambers pre-coated with 100 μg ml^{-1} FN or ICAM-1. After 4 h, migrated cells were counted in five randomly selected high power fields (×400) per well. Results were expressed as mean + SD per mm^2 from one representative experiment. Results are representative of three independent experiments for (A), (B) and (C), respectively. SM+, Jurkat-SM+ cells; SM/kd, Jurkat-SMS1/kd cells.

in size even though TCR were clustered (Fig. 2B). A time course study showed that TCR/rafts clustering in Jurkat-SM+ cells were 62 and 90% for 5 and 15 min, respectively, and that those in Jurkat-SMS1/kd cells were 15 and 30%, respectively (Fig. 2C). These results indicate that TCR/rafts clustering was severely impaired in Jurkat-SMS1/kd cells compared with Jurkat-SM+ cells.

Roles of membrane SM in CD3-mediated T cell activation

To address our hypothesis that membrane SM has a role in T cell activation, cells were stimulated with 1 μg ml^{-1} of anti-CD3 mAb (OKT3) for 6, 24, 48, 60 and 72 h, and cellular expression of CD69, the earliest leukocyte activation marker (37), was analyzed by FACS. CD69 expression on Jurkat-SMS1/kd cells was markedly decreased over the time course of the assay compared with that on Jurkat-SM+ cells (Fig. 3A). We also examined the effect of PMA, a direct PKC activator, on expression of CD69 in Jurkat-SMS1/kd and Jurkat-SM+ cells. Although CD69 expression induced by CD3 cross-linking was markedly decreased in Jurkat-SMS1/kd cells, similar levels of CD69 were induced by PMA on both cell types (Fig. 3B). These results suggest that membrane SM is involved in TCR/CD3-mediated CD69 expression.

Activation of T cells through the CD3–TCR complex or phorbol esters results in a rapid increase of cell adhesion through integrin receptor activation (24, 38). Therefore, we examined adhesion of Jurkat-SMS1/kd and Jurkat-SM+ cells to FN after CD3/TCR activation or PMA stimulation. As shown in Fig. 3(C), CD3 cross-linking as well as PMA stimulation dramatically enhanced adhesion of Jurkat-SM+ cells to FN compared with only a marginal increase in Jurkat-SMS1/kd cells. We also examined migration of Jurkat-SMS1/kd and Jurkat-SM+ cells in response to stromal cell-derived factor 1α (CXCL12) using transwell chambers pre-coated with FN or ICAM-1. In contrast to cell adhesion, migration of

both cells was equally enhanced in response to CXCL12 (Fig. 3D). These results indicate that TCR-independent functions of Jurkat-SMS1/kd cells are normal.

Role of membrane SM in TCR-mediated signal transduction

Lipid raft-associated adapter protein LAT, is an anchor molecule for TCR signals, via phosphotyrosine-based docking motifs (6). We examined tyrosine phosphorylation of LAT and *ZAP-70* following CD3/TCR stimulation of Jurkat-SM+ and Jurkat-SMS1/kd cells. As shown in Fig. 4, CD3 stimulation induced marked tyrosine phosphorylation of LAT (Fig. 4A) and *ZAP-70* (Fig. 4B) in Jurkat-SM+ cells, while phosphorylation was severely impaired in Jurkat-SMS1/kd cells.

LAT contains multiple tyrosine-based motifs which are phosphorylated by *ZAP-70* or *Syk* and initiates assembly with SH2 domain-containing signaling proteins such as PI3K, PLCγ1 and Grb2, allowing extension of the signaling scaffold (39–42). Immunoblotting analysis revealed that the 72 and 25 kDa proteins were *ZAP-70* and Grb2, respectively. Association of LAT with *ZAP-70* and Grb2 was severely decreased in Jurkat-SMS1/kd cells (Fig. 4C).

Since PKCθ is the major isoform of PKC that locates into the immunological synapse and mediates NF-κB activation after CD3/CD28 stimulation (10, 43), we examined the phosphorylation of PKCθ after CD3 stimulation of Jurkat-SMS1/kd and Jurkat-SM+ cells. Cells were stimulated with the indicated concentration of CD3 mAb for 15 min (Fig. 4D) or stimulated with 1.0 μg ml^{-1} of CD3 mAb for the indicated time (Fig. 4E). After stimulation, cells were lysed, electrophoresed and subjected to immunoblot with antibody to PKCθ and phospho-PKCθ. Stimulation of Jurkat-SM+ cells with CD3 mAb induced phosphorylation of PKCθ, whereas Jurkat-SMS1/kd cells contained no detectable phosphorylated PKCθ (Fig. 4D and E).

Role of membrane SM in translocation of signaling molecules and TCR into lipid rafts

It is well known that TCR engagement induces the translocation of the TCR complex and multiple other signaling molecules such as ZAP-70, Vav, SLP-76, PLCγ1 and PKCθ into lipid rafts (4, 5, 44). Therefore, we investigated whether the distribution of signaling molecules and TCR in rafts are different in Jurkat-SMS1/kd compared with Jurkat-SM+ cells following CD3 cross-linking. Lipid rafts were isolated using equilibrium sucrose density gradients as described (17). The position of the membrane rafts in the sucrose gradient was determined by the presence of *lck* and LAT as well as a well-established raft-associated marker, ganglioside GM1. As shown in Fig. 5(A), *lck*, LAT and ganglioside GM1 were enriched in the upper part of the sucrose gradient (fractions 4 and 5), indicating a separation of the lipid rafts from the Triton X-100-soluble membrane. Although *ZAP-70* and phospho-PKCθ were detected in raft fractions of Jurkat-SMS1/kd and Jurkat-SM+ cells prior to stimulation, a substantial activation-induced shift of *ZAP-70* and PKCθ into raft fractions was observed in Jurkat-SM+ cells. In contrast, translocation of *ZAP-70* and PKCθ was severely impaired in Jurkat-SMS1/kd cells (Fig. 5A). We examined the redistribution of TCR,

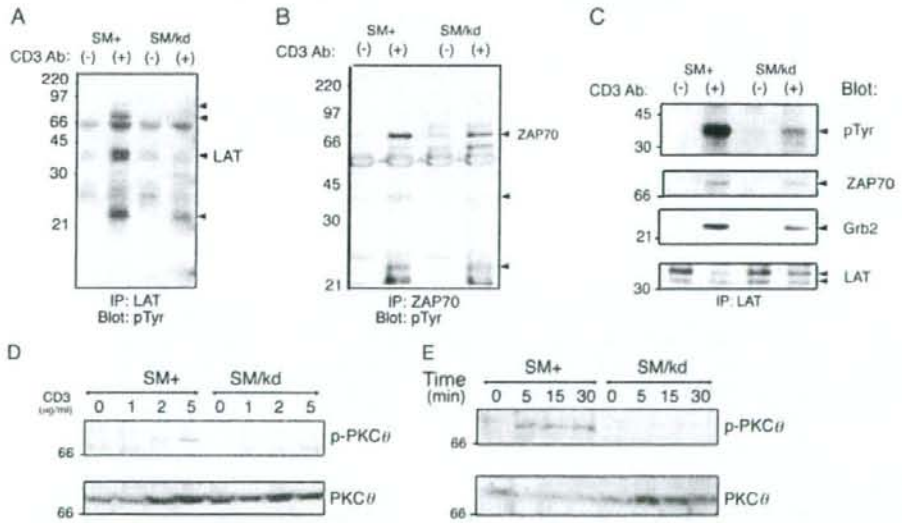

Fig. 4. Role of membrane SM on TCR-mediated signal transduction. Tyrosine phosphorylation of LAT (A) and *ZAP-70* (B). Jurkat-SM+ and Jurkat-SMS1/kd cells were stimulated in the presence or absence of 2 μg ml^{-1} of CD3 mAb for 5 min. LAT and *ZAP-70* were immunoprecipitated and subjected to SDS–PAGE and anti-phosphotyrosine immunoblotting. (C) Association of LAT with *ZAP-70* and Grb2. LAT was immunoprecipitated and subjected to anti-phosphotyrosine (p-Tyr), anti-ZAP-70, anti-Grb2 and anti-LAT immunoblotting. (D) Dose dependency of CD3 mAb on phosphorylation of PKCθ. (E) Time course of PKCθ phosphorylation. Cells were stimulated with the indicated concentration of CD3 mAb for 15 min (D) or stimulated with 5.0 μg ml^{-1} of CD3 mAb for the indicated time (E). After stimulation, cells were lysed and proteins were analyzed by immunoblotting with antibody to PKCθ and phospho-PKCθ (p-PKCθ). These data are representative of more than five independent experiments for (A), (B) and (C) and three independent experiments for (D) and (E), respectively. SM+, Jurkat-SM+ cells; SM/kd, Jurkat-SMS1/kd cells.

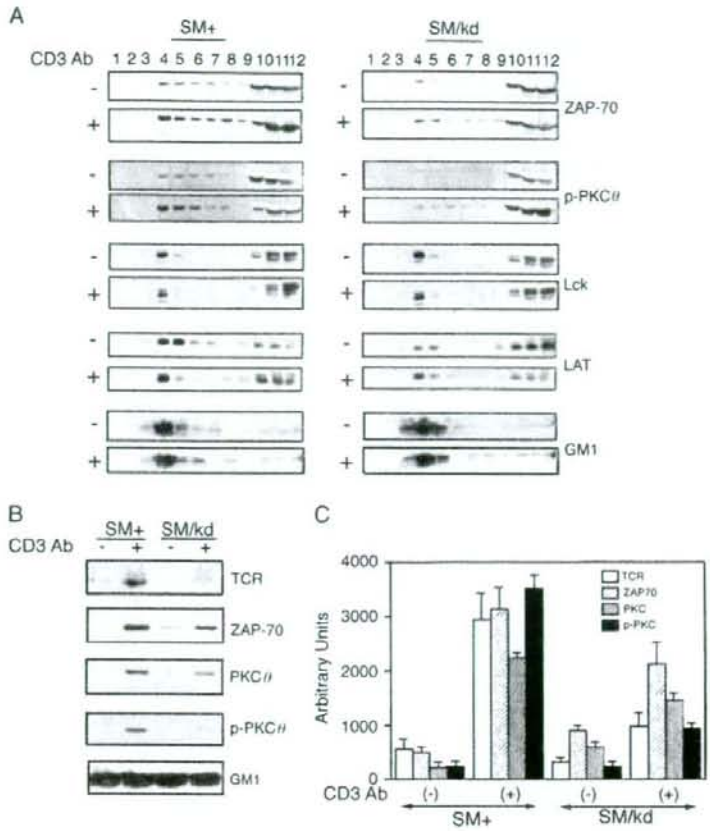

Fig. 5. Role of membrane SM in translocation of signaling molecules into lipid rafts. (A) Lipid rafts fractionation. Cells (2.5×10^8) were left unstimulated (-) or were stimulated with anti-OKT3 mAb for 5 min (+) and Triton X lysates were subjected to sucrose density gradient fractionation. Fractions were run on 15% SDS–PAGE and immunoblotted with antibodies against *ZAP-70*, p-PKCθ and markers for the raft fractions, Lck, LAT and ganglioside GM1. The blots shown are representative of four independent experiments. (B) Redistribution of TCR, *ZAP-70*, PKCθ, p-PKCθ into lipid rafts upon CD3 stimulation. Raft fractions (mixtures of fraction 4 and 5) were run on 15% SDS–PAGE and immunoblotted with the indicated antibodies. (C) Quantification of TCR, *ZAP-70*, PKCθ, p-PKCθ in lipid rafts. Quantification of each band was performed densitometrically using NIH image software and normalized to the amount of ganglioside GM1. Data are average ± SD of three independent experiments and expressed as the arbitrary units.

ZAP-70 and phospho-PKCθ in the raft fractions (fractions 4 and 5) before and after CD3 stimulation several times and compared their translocation in Jurkat-SMS1/kd and Jurkat-SM+ cells (Fig. 5B). As shown in Fig. 5(C), we found that translocation of these signaling molecules is significantly inhibited in Jurkat-SMS1/kd cells compared with Jurkat-SM+ cells after CD3 stimulation.

Discussion

For full T cell activation, the lateral organization of membrane-associated proteins such as the TCR–CD3 complex, PTKs and adaptor molecules are required to sustain the activation signals (8, 11). It has been suggested that sphingolipid- and cholesterol-rich microdomains, lipid rafts, play a key role in protein sorting, signal transduction and cytoskeletal organization to form platforms at the plasma membrane for TCR signaling (1, 3, 5, 6). Raft functions have been analyzed by either disrupting rafts using the cholesterol-chelating reagent, MβCD, or by disrupting the targeting of signaling proteins to rafts. To examine the role of major rafts component, SM, in T cell function, we established the membrane SM-deficient cell line, Jurkat-SMS1/kd, by transfection of *SMS1*-siRNA into Jurkat T cells. *SMS1* gene copy number and SMS activity were decreased in the Jurkat-SMS1/kd cells to ~60% of Jurkat-SM+ cells (Fig. 1A and B). However, reduction in SM levels in Jurkat-SMS1/kd cells was only minor (23%) compared with Jurkat-SM+ cells (Fig. 1C). This discrepancy may be explained by uptake of SM from serum into the medium. An alternative explanation could be that *SMS2* and *SMSr* may substitute SMS levels. Reduction of SMS activity and membrane SM levels in Jurkat-SMS1/kd cells are similar to those in *SMS1*-siRNA-treated cells previously reported (45, 46).

It has been reported that lysenin specifically binds SM only when SM is in the form of a cluster (33). Jurkat-SMS1/kd cells

were negative for lysenin staining (Fig. 1F and G) and resistant to lysenin-mediated lysis (Fig. 1D and E). Although cellular SM levels were not markedly different, we consider the membrane SM level strongly decreased in Jurkat-SMS1/kd cells. Using this system, we found that CD3-induced tyrosine phosphorylation of LAT and threonine phosphorylation of PKCθ were severely inhibited in Jurkat-SMS1/kd cells compared with those in Jurkat-SM+ cells (Fig. 4A, D and E). Moreover, decreased tyrosine phosphorylation of LAT was accompanied by decreased association of *ZAP-70* and Grb2 (Fig. 4C). These inhibitions may result in impaired CD3-mediated cellular activation, such as decreased CD69 expression and cell adhesion to FN in Jurkat-SMS1/kd cells (Fig. 3A–C), suggesting that membrane SM has an important role in T cell activation. In contrast, PMA enhanced CD69 expression equally on both Jurkat-SMS1/kd and Jurkat-SM+ cells (Fig. 3B) and migration of both cells was equally enhanced in response to CXCL12 (Fig. 3D). Therefore, raft-independent functions of Jurkat-SMS1/kd cells were considered to be normal, in spite of the fact that contents of SM metabolites like ceramide, sphingosine and sphingosine 1-phosphate may change and have some effects on cellular functions.

Since lipid raft-resident molecules such as *src* family kinases and the ganglioside GM1 relocalize toward the immunological synapse, it appears that the immunological synapse might be described as a large merger of lipid rafts. However, the initial signals during T cell activation, such as tyrosine phosphorylation, calcium mobilization and phosphoinositide metabolism, occur much earlier than immunological synapse formation (47, 48), and TCR-induced activation of *ZAP-70* by *lck* reaches its maximum even before the typical cSMAC has been formed (47). In addition, TCR-mediated tyrosine kinase signaling occurs primarily at the periphery of the synapse (47, 49), suggesting that spatial-temporal activation may regulate immunological synapse formation (50). Recently, Yokosuka *et al.* (12) have reported that microclusters consisting of CD3ζ, *ZAP-70* and SLP-76 were generated continuously at the periphery of immunological synapses and that TCRs at the contact sites were translocated into the cSMAC, whereas most *ZAP-70* and SLP-76 molecules did not move to the cSMAC. Varma *et al.* (13) also reported that TCR signaling is sustained by stabilized microclusters and is terminated in the cSMAC. Both reports suggested that the cSMAC may function in mediating the microcluster-induced stop signal or TCR degradation. However, these reports do not contradict the existence of rafts or their functions for the following reasons. Estimated raft size in resting cells is between 50 and 200 nm, and there is heterogeneity in the partitioning of the proteins residing in rafts. For example, cholesterol extraction destabilizes the membrane microdomains containing *lck*, but not LAT (51). Recently, Nicolau *et al.* have reported that dynamic partitioning into rafts increases specific interprotein collision rates to maximize the biologically relevant function. Therefore, lipid rafts function as reaction chambers that facilitate nanoscale protein–protein interaction (52). These highly dynamic spatial confinements result in a high probability of raft-targeted molecule species to come into the vicinity with each other but with rapidly exchanging individual molecules. Therefore, many tyrosine phosphorylated proteins become concentrated in the rafts at periphery of immunological synapse upon TCR stimulation. It has been reported that these tyrosine phosphorylated proteins including the TCR–CD3 receptor complex, especially hyper-phosphorylated CD3ζ chains, ZAP-70, PLCγ, Vav and Shc, are detected mainly in rafts by biochemical separation. Consistent with previous reports, we found that translocation of TCR, *ZAP-70* and PKCθ into raft fractions was observed in Jurkat-SM+ cells, but was severely impaired in Jurkat-SMS1/kd cells (Fig. 5), suggesting an important role of membrane SM as a lipid raft constituent enabling translocation of signaling molecules into lipid rafts.

Lipid rafts also stabilize and amplify signals resulting from aggregation of rafts to larger complexes, which are accompanied by further recruitment of important signaling mediators such as LAT and associated molecules and TCR components. In this regard, we have previously reported that membrane SM is crucial for Fas/lipid rafts clustering through local ceramide production that may compartmentalize lipid rafts to ceramide-enriched membrane platforms (17). In addition to this mechanism, functional links between the cytoskeletal machinery and lipid rafts seem important for forming signaling platforms, such as the immunological synapse. Membrane rafts appear to be the place where TCRs become associated with actin cytoskeleton (53–55), since disruption of lipid rafts by MβCD abolished the association of the ζ chain with the actin cytoskeleton. Among intermediate actin-binding proteins, the ezrin–radixin–moesin family of proteins associate with lipid rafts and their binding to actin filaments and membrane proteins is regulated by PKCθ that is recruited to the immunological synapse on stimulation (10, 43). In this study, we clearly demonstrate that translocation of PKCθ was severely decreased in Jurkat-SMS1/kd cells (Fig. 5). This decrease may account for impaired TCR/CD3 clustering in Jurkat-SMS1/kd cells (Fig. 2).

Thus, lipid rafts may not only facilitate distinct protein–protein interactions to build signaling complexes by increasing their local concentration and the probability of contacting and interacting with signaling molecules but also form signaling platforms by cytoskeleton-driven events. Segregation of the plasma membrane into distinct domains is an essential element of immune cell activation and dynamic properties of the membrane depend strongly on the lipid composition (56). Changes in lipid composition are shown to alter the distribution of raft-resident proteins (57). Taken altogether, our data indicate that membrane SM is an important component of lipid rafts and crucial for various raft functions.

Funding

Japanese Ministry of Education and Science and Culture, Uehara Memorial Foundation and Kanazawa Medical University Research Foundation (13557160, 15024236, 15390313, 13877075, 15024236, 15390313); JSPS Grant-in-Aid research funds and Uehara Memorial Foundation to Z.-X.J.

Acknowledgements

Authors dedicate this manuscript to Dr E.T.B. and mourn over her unexpected death.

Abbreviation

cSMAC	central supramolecular activation cluster
CTx	cholera toxin B
FN	fibronectin
fPEG-Chol	fluorescein ester of poly(ethyleneglycol)-derivatized cholesterol ether
FRET	fluorescence resonance energy transfer
GAPDH	glyceraldehyde 3-phosphate dehydrogenase
HSA	human serum albumin
ICAM	inter cellular adhesion molecules
LAT	linker for activation of T cell
MBP	maltose-binding protein
MBS	MS-buffered saline
MβCD	methyl-β-cyclodextrin
PI3K	phosphatidylinositol 3 kinase
PKC	protein kinase C
PLC-γ	phospholipase C_γ
PMA	phorbol myristate acetate
PMSF	phenylmethylsulfonyl fluoride
PTK	protein tyrosine kinase
SCR	scrambled sequence
siRNA	short-interfering RNA
SM	sphingomyelin
SMS	sphingomyelin synthase
TLC	thin-layer chromatography

References

1 Simons, K. and Ikonen, E. 1997. Functional rafts in cell membranes. *Nature* 387:569.
2 Cherukuri, A., Dykstra, M. and Pierce, S. K. 2001. Floating the raft hypothesis: lipid rafts play a role in immune cell activation. *Immunity* 14:657.
3 Alonso, M. A. and Millan, J. 2001. The role of lipid rafts in signalling and membrane trafficking in T lymphocytes. *J. Cell. Sci.* 114:3957.
4 Munro, S. 2003. Lipid rafts: elusive or illusive? *Cell* 115:377.
5 Dykstra, M., Cherukuri, A., Sohn, H. W., Tzeng, S.-J. and Pierce, S. K. 2003. Location is everything: lipid rafts and immune cell signaling. *Annu. Rev. Immunol.* 21:457.
6 Viola, A. 2001. The amplification of TCR signaling by dynamic membrane microdomains. *Trends Immunol.* 22:322.
7 Zhang, W., Trible, R. P. and Samelson, L. E. 1998. LAT palmitoylation: its essential role in membrane microdomain targeting and tyrosine phosphorylation during T cell activation. *Immunity* 9:239.
8 Samelson, L. E. 2002. Signal transduction mediated by the T cell antigen receptor: the role of adapter proteins. *Annu. Rev. Immunol.* 20:371.
9 Sun, Z., Arendt, C. W., Ellmeier, W. *et al.* 2000. PKC-θ is required for TCR-induced NF-κB activation in mature but not immature T lymphocytes. *Nature* 404:402.
10 Bi, K., Tanka, Y., Coudronniere, N. *et al.* 2001. Antigen-induced translocation of PKC-theta to membrane rafts is required for T cell activation. *Nat. Immunol.* 2:556.
11 Bromley, S. K., Burack, W. R., Johnson, K. G. *et al.* 2001. The immunological synapse. *Annu. Rev. Immunol.* 19:375.
12 Yokosuka, T., Sakata-Sogawa, K., Kobayashi, W. *et al.* 2005. Newly generated T cell receptor microclusters initiate and sustain T cell activation by recruitment of Zap70 and SLP-76. *Nat. Immunol.* 6:1253.
13 Varma, R., Campi, G., Yokosuka, T., Saito, T. and Dustin, M. L. 2006. T cell receptor-proximal signals are sustained in peripheral microclusters and terminated in the central supramolecular activation cluster. *Immunity* 25:117.
14 Saito, T. and Yokosuka, T. 2006. Immunological synapse and microclusters: the site for recognition and activation of T cells. *Curr. Opin. Immunol.* 18:305.
15 Yamaoka, S., Miyaji, M., Kitano, T., Umehara, H. and Okazaki, T. 2004. Expression cloning of a human cDNA restoring sphingomyelin synthesis and cell growth in sphingomyelin synthase-deficient cells. *J. Biol. Chem.* 279:18688.
16 Huitema, K., van den Dikkenberg, J., Brouwers, J. F. and Holthuis, J. C. 2004. Identification of a family of animal sphingomyelin synthases. *EMBO J.* 23:33.
17 Miyaji, M., Jin, Z. X., Yamaoka, S. *et al.* 2005. Role of membrane sphingomyelin and ceramide in platform formation for Fas-mediated apoptosis. *J. Exp. Med.* 202:249.
18 Jin, Z., Kishi, H., Wei, X., Matsuda, T., Saito, S. and Muraguchi, A. 2002. Lymphoid enhancer-binding factor-1 binds and activates the recombination-activating gene-2 promoter together with c-Myb and Pax-5 in immature B cells. *J. Immunol.* 167:3783.
19 Yamaji-Hasegawa, A., Makino, A., Baba, T. *et al.* 2003. Oligomerization and pore formation of a sphingomyelin-specific toxin, lysenin. *J. Biol. Chem.* 278:22762.
20 Sato, S. B., Ishii, K., Makino, A. *et al.* 2004. Distribution and transport of cholesterol-rich membrane domains monitored by a membrane-impermeant fluorescent polyethylene glycol-derivatized cholesterol. *J. Biol. Chem.* 279:23790.
21 Inoue, H., Yoneda, C., Minami, Y. *et al.* 2002. Lipid rafts as the signaling scaffold for NK cell activation: tyrosine phosphorylation and association of LAT with PI 3-kinase and PLC-γ following CD2 stimulation. *Eur. J. Immunol.* 32:2160.
22 Goda, S., Imai, T., Yoshie, O. *et al.* 2000. CX3C-chemokine, fractalkine enhanced adhesion of THP-1 cells to endothelial cells through integrin-dependent and independent mechanisms. *J. Immunol.* 164:4313.
23 Gouda, S., Inoue, H., Umehara, H. *et al.* 2006. Matrix metalloproteinase-1 produced by human CXCL12-stimulated natural killer cells. *Am. J. Pathol.* 169:445.
24 Goda, S., Quale, A. C., Woods, M. L., Felthauser, A. and Shimizu, Y. 2004. Control of TCR-mediated activation of b1 integrins by the ZAP-70 tyrosine kinase interdomain B region and the linker for activation of T cells adapter protein. *J. Immunol.* 172:5379.
25 Okazaki, T., Bell, R. M. and Hannun, Y. A. 1989. Sphingomyelin turnover induced by vitamin D3 in HL-60 cells. *J. Biol. Chem.* 264:19076.
26 Umehara, H., Huang, J.-Y., Kono, T. *et al.* 1997. Involvement of protein tyrosine kinase p72syk and phosphatidylinositol 3-kinase in CD2-mediated granular exocytosis in natural killer cell line. *J. Immunol.* 159:1200.
27 Takagi, S., Tojo, H., Tomita, S. *et al.* 2003. Alteration of the 4-sphingenine scaffolds of ceramides in keratinocyte-specific Arnt deficient mice affects skin barrier function. *J. Clin. Invest.* 112:1372.
28 Nagatsuka, Y., Tojo, H. and Hirabayashi, Y. 2006. Identification and analysis of novel glycolipids in vertebrate brains by HPLC/mass spectrometry. *Methods Enzymol.* 417:155.
29 Han, X. and Gross, R. 2001. Quantitative analysis and molecular species fingerprinting of triacylglyceride molecular species directly from lipid extracts of biological samples by electrospray ionization tandem mass spectrometry. *Anal. Biochem.* 295:88.
30 Umehara, H., Huang, J.-Y., Kono, T. *et al.* 1998. Co-stimulation of T cells with CD2 augments TCR-CD3-mediated activation of protein tyrosine kinase p72syk, resulting in increased tyrosine phosphorylation of adapter proteins Shc and Cbl. *Int. Immunol.* 10:833.
31 Taguchi, Y., Kondo, T., Watanabe, M. *et al.* 2004. Interleukin-2-induced survival of natural killer (NK) cells involving phosphatidylinositol-3 kinase-dependent reduction of ceramide through acid sphingomyelinase, sphingomyelin synthase and glucosylceramide synthase. *Blood* 104:3285.
32 Yamaji, A., Sekizawa, Y., Emoto, K. *et al.* 1998. Lysenin, a novel sphingomyelin-specific binding protein. *J. Biol. Chem.* 273:5300.
33 Kobayashi, T., Takahashi, M., Nagatsuka, Y. and Hirabayashi, Y. 2006. Lipid rafts: new tools and a new component. *Biol. Pharm. Bull.* 29:1526.
34 Kiyokawa, E., Baba, T., Otsuka, N., Makino, A., Ohno, S. and Kobayashi, T. 2005. Spatial and functional heterogeneity of sphingolipid-rich membrane domains. *J. Biol. Chem.* 280:24072.
35 Davis, D. M. and Dustin, M. L. 2004. What is the importance of the immunological synapse? *Trends Immunol.* 25:323.
36 Rodgers, W., Farris, D. and Mishra, S. 2005. Merging complexes: properties of membrane raft assemble during lymphocyte signaling. *Trends Immunol.* 26:97.

37 Sancho, D., Gomez, M. and Sanchez-Madrid, F. 2005. CD69 is an immunoregulatory molecule induced following activation. *Trends Immunol.* 26:136.
38 Dustin, M. L., Bivona, T. G. and Philips, M. R. 2004. Membranes as messengers in T cell adhesion signaling. *Nat. Immunol.* 5:363.
39 Tomlinson, M. G., Lin, J. and Weiss, A. 2000. Lymphocytes with a complex: adapter proteins in antigen receptor signaling. *Immunol. Today* 21:584.
40 Rudd, C. E. 1999. Adaptors and molecular scaffolds in immune cell signaling. *Cell* 96:5.
41 van Oers, N. S. C. 1999. T cell receptor-mediated signs and signals governing T cell development. *Semin. Immunol.* 11:227.
42 van Leeuwen, J. E. M. and Samelson, L. E. 1999. T cell antigen-receptor signal transduction. *Curr. Opin. Immunol.* 11:242.
43 Huang, J., Lo, P.-F., Zal, T. *et al.* 2002. CD28 plays a critical role in the segregation of PKCθ within the immunologic synapse. *Proc. Natl Acad. Sci. USA* 99:9369.
44 Harder, T. 2004. Lipid raft domains and protein networks in T-cell receptor signal transduction. *Curr. Opin. Immunol.* 16:353.
45 Li, Z., Hailemariam, T. K., Zhou, H. *et al.* 2007. Inhibition of sphingomyelin synthase (SMS) affects intracellular sphingomyelin accumulation and plasma membrane lipid organization. *Biochim. Biophys. Acta* 1771:1184.
46 Tafesse, F. G., Huitema, K., Hermansson, M. *et al.* 2007. Both sphingomyelin synthases SMS1 and SMS2 are required for sphingomyelin homeostasis and growth in human HeLa cells. *J. Biol. Chem.* 282:17537.
47 Lee, K.-H., Holdorf, A. D., Dustin, M. L., Chan, A. C., Allen, P. M. and Shaw, A. S. 2002. T cell receptor signaling precedes immunological synapse formation. *Science* 295:1539.
48 Irvine, D., Purbhoo, M., Krogsgaard, M. and Davis, M. 2002. Direct observation of ligand recognition by T cells. *Nature* 419:845.
49 Freiberg, B. A., Kupfer, H., Maslanik, W. *et al.* 2002. Staging and resetting T cell activation in SMACs. *Nat. Immunol.* 3:911.
50 Mossman, K. D., Campi, G., Groves, J. T. and Dustin, M. L. 2005. Altered TCR signaling from geometrically repatterned immunological synapses. *Science* 310:1191.
51 Schade, A. E. and Levine, A. D. 2002. Lipid raft heterogeneity in human peripheral blood T lymphoblasts: a mechanism for regulating the initiation of TCR signal transduction. *J. Immunol.* 168:2233.
52 Nicolau, D. V. J., Burrage, K., Parton, R. G. and Hancock, J. F. 2006. Identifying optimal lipid raft characteristics required to promote nanoscale protein-protein interactions on the plasma membrane. *Mol. Cell. Biol.* 26:313.
53 Dustin, M. L. and Cooper, J. A. 2000. The immunological synapse and the actin cytoskeleton: molecular hardware for T cell signaling. *Nat. Immunol.* 1:23.
54 Hogg, N., Laschinger, M., Giles, K. and McDowall, A. 2003. T-cell integrins: more than just sticking points. *J. Cell Sci.* 116:4695.
55 Zeyda, M. and Stulnig, T. M. 2006. Lipid rafts & Co.: an integrated model of membrane organization in T cell activation. *Prog. Lipid Res.* 45:187.
56 Harder, T., Rentero, C., Zech, T. and Gaus, K. 2007. Plasma membrane segregation during T cell activation: probing the order of domains. *Curr. Opin. Immunol.* 19:470.
57 Garner, A. E., Smith, D. A. and Hooper, N. M. 2007. Sphingomyelin chain length influences the distribution of GPI-anchored proteins in rafts in supported lipid bilayers. *Mol. Membr. Biol.* 24:233.

M8:00158-JLR

Synthesis of 2-hydroxy-ceramide by ceramide synthase family members: enzymatic basis for the preference of fatty acid chain length in cultured cell models

Yukiko Mizutani,* Akio Kihara,†,§ Hiroko Chiba,* Hiromasa Tojo,** and Yasuyuki Igarashi*,†,1

Laboratory of Biomembrane and Biofunctional Chemistry,* Faculty of Advanced Life Sciences, Hokkaido University, Kita 21-jo, Nishi 11-choume, Kita-ku, Sapporo 001-0021, Japan; Laboratory of Biomembrane and Biofunctional Chemistry,† Faculty of Pharmaceutical Sciences, Hokkaido University, Kita 12-jo, Nishi 6-choume, Kita-ku, Sapporo 060-0812, Japan; Laboratory of Biochemistry,§ Faculty of Pharmaceutical Sciences, Hokkaido University, Kita 12-jo, Nishi 6-choume, Kita-ku, Sapporo 060-0812, Japan; and Department of Biochemistry and Molecular Biology,** Osaka University Graduate School of Medicine, 2-2 Yamadaoka, Suita, Osaka 565-0871, Japan

Abbreviated title: Synthesis of 2-hydroxy-CER by CerS/LASS

[1]To whom correspondence should be addressed.
Yasuyuki Igarashi, Ph.D.
Laboratory of Biomembrane and Biofunctional Chemistry, Faculty of Advanced Life Sciences, Hokkaido University, Kita 21-jo, Nishi 11-choume, Kita-ku, Sapporo 001-0021, Japan.
Phone: +81-11-706-9001, Fax: +81-11-706-9024
E-mail: yigarash@pharm.hokudai.ac.jp

Abbreviations: CER, ceramide; CerS, ceramide synthase; FA, fatty acid; LASS, longevity assurance homologue; LCB, long-chain base; RT, reverse transcription; Sph, sphingosine; C18:0, stearoyl; MS/MS, tandem mass spectrometry.

Abstract

Ceramide is unusually abundant in epidermal stratum corneum and is important for permeability barrier function. Ceramides in epidermis also comprise an unusual variety, including 2-hydroxy (α-hydroxy)-ceramide. Six mammalian CerS/LASS family members have been identified as synthases responsible for ceramide production. We reveal here that, of the six, *CerS3/LASS3* mRNA is the most predominantly expressed in keratinocytes. Moreover, its expression is increased upon differentiation. CerS family members have known substrate specificities for fatty acyl-CoA chain length and saturation, yet their abilities to produce 2-hydroxy-ceramide have not been examined. In the presented study, we demonstrate that all CerS members can produce 2-hydroxy-ceramide when overproduced in HEK 293T cells. Each produced a 2-hydroxy-ceramide with a chain length similar to that of the respective non-hydroxy-ceramide produced. In HeLa cells overproducing the fatty acid 2-hydroxylase FA2H, knock-down of *CerS2* resulted in a reduction in total long-chain 2-hydroxy-ceramides, confirming enzyme substrate specificity for chain length. *In vitro* ceramide synthase assays confirmed the ability of CerS1 to utilize 2-hydroxy-stearoyl-CoA as a substrate. These results suggest that all CerS members can synthesize 2-hydroxy-ceramide with specificity for 2-hydroxy-fatty acyl-CoA chain length and that CerS3 may be important in ceramide and 2-hydroxy-ceramide synthesis in epidermis.

Supplementary key words: ceramide, ceramide synthase, epidermis, fatty acid hydroxylase.

INTRODUCTION

Sphingolipids are essential lipid components of the eukaryotic plasma membrane. The hydrophobic backbone of sphingolipids, ceramide (CER), functions in cellular signaling during such processes as apoptosis, cell differentiation, and cell cycle arrest (1, 2). In epidermal stratum corneum, CER is a major lipid component and is important for epidermal permeability barrier formation (3, 4).

CER consists of a fatty acid (FA) and an amide-linked long-chain base (LCB). In mammals, FA chain length typically ranges from 14-26 carbons (C14 to C26), with the C16 (C16:0) and C24 (C24:0 and C24:1) species being predominant in most tissues. FAs in CER are typically non-hydroxylated, although in certain tissues, including skin and brain, α-hydroxy (2-hydroxy) FAs are abundant (5, 6). In these tissues, 2-hydroxy-FA is converted from free FA by the hydroxylase FA2H (7, 8), which is also known to be induced during keratinocyte differentiation (9). In addition, skin contains ω-hydroxy FA, with a chain length of 30-36, linked to a linoleic acid (C18:2) (10-13).

The major LCB in mammals is sphingosine (Sph), which carries a *trans* double bond between the C-4 and C-5 positions, although dihydrosphingosine (dihydro-Sph), which lacks the double bond, also exists. In addition, phytosphingosine (phyto-Sph), containing a hydroxyl group at the C-4 position, is detectable in certain tissues including skin, small intestine, and kidney (14-16); skin also contains a unique LCB, 6-hydroxy-sphingosine (6-hydroxy-Sph) (17). Thus, due to the diverse species of LCBs and FA's available, skin contains unusually varied CER types. In fact, in the human stratum corneum of epidermis, ten subclasses of CERs have been identified, which

differ in their LCB (Sph, phyto-Sph, and 6-hydroxy-Sph) and FA (non-hydroxy, 2-hydroxy, ω-hydroxy linked to a linoleic acid) species (4, 10-13).

In *de novo* sphingolipid biosynthesis, dihydro-CER is synthesized from dihydro-Sph and fatty acyl-CoA by CER synthase. The dihydro-Sph portion of dihydro-CER is then desaturated by the Δ4-desaturase DES1, creating CER with a Sph moiety (18). Alternatively, in certain tissues including skin, the C4-hydroxylase DES2 produces CER with a phyto-Sph (phyto-CER) (19-21). CERs can also be produced by the salvage pathway, in which Sph generated by the deacylation of CER is re-acylated by CER synthase.

There are six mammalian CER synthases: ceramide synthase (CerS)1/longevity assurance homologue (LASS)1, CerS2/LASS2, CerS3/LASS3, CerS4/LASS4, CerS5/LASS5, and CerS6/LASS6 (22). These enzymes share high sequence similarity and together constitute the CerS family. Each CerS member exhibits a characteristic fatty acyl-CoA preference (CerS1, C18; CerS2, C22 and C24; CerS4, C20, C22 and C24; and CerS5 and CerS6, C16), with the exception of CerS3, which exhibits broad substrate specificity toward medium- to long-chain fatty acyl-CoAs (short-chain having ≤C18; medium-chain, C18-C22; and long-chain, ≥C22) (23-28).

CerS members also exhibit substrate preference with regards to the saturation of the fatty acyl-CoA. For example, CerS1, CerS4, and CerS6 can use C18:0-CoA but not C18:1-CoA as a substrate (26). However, the substrate preference of CerS members regarding 2-hydroxy-fatty acyl-CoA has not yet been examined. Therefore, in the present study we tested the ability of each CerS member to produce 2-hydroxy-CER

(CER containing 2-hydroxy-FA). In *in vivo* metabolic labeling experiments and *in vitro* CER synthase assays all CerS members produced 2-hydroxy-CER with efficiency similar to that observed for their synthesis of non-hydroxy-CER. Furthermore, the expression of CerS3 and CerS4 was found to increase during keratinocyte differentiation, while the expression levels of other CerS family members remained mostly unchanged. These data suggest that differing expression patterns for CerS family members play important roles in the production of unique epidermal CERs, including 2-hydroxy-CER.

MATERIALS AND METHODS

Cell culture and transfection

Normal human epidermal keratinocytes isolated from neonatal skin were obtained from Cambrex (Walkersville, MD), and were grown in a serum-free keratinocyte growth medium (Invitrogen, Carlsbad, CA) containing 0.07 mM calcium. Keratinocyte differentiation was performed as described previously (21) using differentiation medium (Dulbecco's modified Eagle's medium and Ham's F-12 medium (2:1, v/v), supplemented with 1.3 mM calcium, 10% FBS, 10 μg/ml insulin, 0.4 μg/ml hydrocortisone, and 50 μg/ml vitamin C).

Human embryonic kidney (HEK) 293T cells and HeLa cells were grown in Dulbecco's modified Eagle's medium containing 10% FBS and supplemented with 100 units/ml penicillin and 100 μg/ml streptomycin. HEK 293T cells were grown in culture dishes coated with 0.3% collagen. Transfections were performed using Lipofectamine

Plus™ Reagent (Invitrogen), according to the manufacturer's manual. Lysates of transiently transfected cells were prepared 24 hr after transfection.

Plasmids

Human *FA2H* cDNA was amplified by RT-PCR using human epidermal keratinocyte total RNA and the primers 5'-GAGATCTATGGCCCCCGCTCCGCCCCCCGC-3' and 5'-TCAGGTGGGGTTTCTCTGGAGTGAGG-3'. The amplified DNA fragment was cloned into pGEM-T Easy vector (Promega, Madison, WI) to generate pGEM FA2H (*Bgl*II). The mammalian expression vector pCE-puro 3xFLAG-1, a derivative of pCE-puro, was constructed to create an N-terminally triple FLAG (3xFLAG)-tagged gene (29). The 1.1 kb *Bgl*II-*Not*I fragment of pGEM-FA2H (*Bgl*II) was cloned into the *Bam*HI-*Not*I site of the pCE-puro 3xFLAG-1 to generate pCE-puro 3xFLAG-FA2H.

The pcDNA3 HA-CerSx plasmids (with x representing the CerS numbers), which encode N-terminally HA-tagged mouse CerS family members, and the pcDNA3 DES2 plasmid encodes untagged human DES2, as described previously (21, 26, 27).

Reverse transcription (RT)-PCR

Total RNA was isolated from cultured cells using an RNeasy Mini Kit (Qiagen), according to the manufacturer's manual. RT-PCR was performed on total RNA using a SuperScript One-Step RT-PCR with Platinum Taq kit (Invitrogen). PCR products were separated by electrophoresis on 1.5% agarose gels and visualized by ethidium bromide

staining. Primers for actin were designed and used as an endogenous control. The following primer sets were used for this assay: *FA2H*, 5'-CAAGGACCTGGTGGACTGGC-3' and 5'-GCTGCATGCACAAGTAGAAGAC-3'; *Keratin 1*, 5'-GGTGGACGTGGTAGTGGCTTTG-3' and 5'-TTCAGTTCCGAATCCAACCGAG-3'; *CerS1*, 5'-ATGCCGAGCTACGCGCAGCTAGTGC-3' and 5'-TTGCGCCAGGTGTCCATGTATAGC-3'; *CerS2*, 5'-CCGTCATTGTGGATAAACCCTG-3' and 5'-GAGGTAGGCCCAGAAGATATG-3'; *CerS3*, 5'-TCAAACATTCCACAAGGCAACC-3' and 5'-AGCAGACTCCAGCCAAATG-3'; *CerS4*, 5'-ATGCTGTCCAGTTTCAACGAG-3' and 5'-AGAGTCTGGTTTGGGTACCTG-3'; *CerS5*, 5'-CAGGGACCCCTAAGCTTGCTG-3' and 5'-CAGCACTGTCGGATGTCCCAG-3'; *CerS6*, 5'-GTGGAATACGAGGCATTGCTG-3' and 5'-ATCATCCTTGGACACCTTGC-3'; and *actin*, 5'-TGATGATATCGCCGCGCTCGTCGTC-3' and 5'-GCATACCCCTCGTAGATGGGCACAG-3'.

Real-time quantitative PCR

Total RNA was isolated from cultured cells using an RNeasy Mini Kit (Qiagen) and converted to cDNA using Affinity Script QPCR cDNA (Stratagen, San Diego, CA) according to the manufacturer's protocol. Real-time quantitative PCR was performed